materials

MDPI

Article

K_2CO_3-Impregnated Al/Si Aerogel Prepared by Ambient Pressure Drying for CO_2 Capture: Synthesis, Characterization and Adsorption Characteristics

Yanlin Wang [1], Baihe Guo [1], Jingnan Guo [1], Man Zhang [2], Hairui Yang [2] and Yan Jin [1,*]

[1] College of Electrical and Power Engineering, Taiyuan University of Technology, Taiyuan 030024, China; 13453122526@163.com (Y.W.); guobaihehappy@163.com (B.G.); gguojingnan@163.com (J.G.)

[2] Department of Energy and Power Engineering, Tsinghua University, Beijing 100000, China; zhangman@mail.tsinghua.edu.cn (M.Z.); yhr@mail.tsinghua.edu.cn (H.Y.)

* Correspondence: jinyan@tyut.edu.cn; Tel.: +86-13934630502

Received: 5 July 2020; Accepted: 18 August 2020; Published: 24 August 2020

Abstract: A new potassium-based adsorbent for CO_2 capture with Al aerogel used as support is proposed in this work. The adsorbents with different surface modifiers (tetraethyl orthosilicate (TEOS) and trimethyl chlorosilane (TMCS)) and different K_2CO_3 loadings (10%, 20%, 30% and 40%) were prepared by sol-gel and iso-volume impregnation processes with ambient pressure drying. The CO_2 adsorption performance of the adsorbents were tested by a fixed-bed reactor, and their adsorption mechanisms were studied by scanning electron microscopy (SEM), Brunauer Emmett Teller (BET), X-ray diffraction (XRD), Fourier transform infrared (FT-IR) spectroscopy, and X-ray fluorescence spectrometry (XRF). Furthermore, the adsorption kinetics and the cycling performance were investigated. The results show that using TEOS to modify the wet gel can introduce SiO_2 to increase the strength of the skeleton. On the basis of TEOS modification, TMCS can further modify –OH, thus effectively avoiding the destruction of aerogel structure during ambient drying and K_2CO_3 impregnation. In this work, the specific surface area and specific pore volume of Al aerogel modified by TEOS + TMCS are up to 635.32 cm^2/g and 2.43 cm^3/g, respectively. The aerogels without modification (Al-B), TEOS modification (Al/Si) and TEOS + TMCS modification (Al/Si-TMCS) showed the best CO_2 adsorption performance at 20%, 30% and 30% K_2CO_3 loading, respectively. In particular, the CO_2 adsorption capacity and K_2CO_3 utilization rate of Al/Si-TMCS-30K are as high as 2.36 mmol/g and 93.2% at 70 degrees Celsius (°C). Avrami's fractional order kinetic model can well fit the CO_2 adsorption process of potassium-based adsorbents. Al-B-20K has a higher apparent activation energy and a lower adsorption rate during the adsorption process. After 15 adsorption-regeneration cycles, Al/Si-TMCS-30K maintain a stable CO_2 adsorption capacity and framework structure, while the microstructure of Al/Si-30K is destroyed, resulting in a decrease in its adsorption capacity by nearly 30%. This work provides key data for the application of Al aerogel in the field of potassium-based adsorbent for CO_2 capture.

Keywords: Al/Si aerogel; surface modification; potassium-based adsorbent; CO_2 adsorption performance; adsorption kinetics

1. Introduction

Global climate change caused by excessive CO_2 emissions has become an indisputable fact [1]. Coal-fired power plants are the largest and most concentrated fixed source of CO_2, and their annual CO_2 emissions account for about 40% of total anthropogenic emissions [2]. Therefore, it is important to develop CO_2 emission reduction technologies applicable to coal-fired power plants.

Post-combustion capture is a relatively mature technology, which is suitable for the removal of CO_2 in the flue gas of traditional coal-fired power plants [3]. At present, the CO_2 capture technology based on the alcohol-amine solution after combustion has achieved large-scale industrial applications [4–6], but its problems of high energy consumption for regeneration, corrosion and amine volatilization cannot be ignored. In contrast, the solid adsorbent can effectively avoid these problems [7]. In recent years, studies on the adsorption characteristics of CO_2 by porous materials such as activated carbon, molecular sieves, carbon nanotubes, and metal organic frameworks (MOFs) have been widely carried out [8–11]. Although some materials have exhibited a good CO_2 adsorption performance under high pressure, the CO_2 adsorption properties of these materials are not satisfactory under normal pressure condition especially in the presence of water vapor: poor selectivity, low adsorption capacity and slow adsorption kinetics.

It has been found that the adsorption performance of porous materials can be improved significantly by loading active components that can interact with CO_2 strongly [12,13]. Amine-based solid adsorbents are one of the most widely studied adsorbents, and its high CO_2 adsorption capacity is widely concerned [14,15]. However, the amine-based adsorbent has many drawbacks such as secondary pollution, loss of active components, and high cost of the adsorbent. In the flue gas environment of the flue downstream of the coal-fired power plant, taking into account the adsorption and regeneration conditions of the adsorbent, the use of relatively inexpensive K_2CO_3 as an active component to capture and separate CO_2 after desulfurization is a potential emission reduction technology [16]. K_2CO_3 can achieve CO_2 adsorption by carbonation reaction, and can be regenerated at a relatively low temperature (120–150 °C). The adsorption and regeneration reaction equations are shown in Equations (1) and (2) [17].

$$K_2CO_3 + CO_2 + H_2O \rightarrow 2KHCO_3 \quad (1)$$

$$2KHCO_3 \rightarrow K_2CO_3 + CO_2 + H_2O \quad (2)$$

Lee et al. [18–21] and Zhao et al. [22–26] conducted in-depth research on the CO_2 adsorption characteristics of supported potassium-based adsorbents. They found that the activity of K_2CO_3 mainly depends on the characteristics of the supports.

Adsorption capacity is an important indicator to measure the CO_2 adsorption performance of potassium-based adsorbent. It directly determines the size of the adsorption equipment required in practical industrial applications, and then determines the cost of the adsorption system. Table 1 summarizes the CO_2 adsorption capacity of potassium-based adsorbents with different supports [26–35], which are relatively low compared to amine-based adsorbents. Due to the limited loading capacity of the support to K_2CO_3, a too high loading will cause the microstructure of the adsorbent to deteriorate, which in turn affects the carbonation activity of the adsorbent [24,25]. Thus, the adsorbent needs to work at a lower loading. The lower loading leads to insufficient CO_2 adsorption capacity of the adsorbent, which is an important factor restricting the adsorption performance of the potassium-based adsorbent.

Table 1. A summary of adsorption capacity of potassium-based adsorbents.

Adsorbents	Loading (%)	Reactor	Reaction Conditions	CO_2 Capture Capacity (mmol/g)	References
K_2CO_3/AC	12.5	Fixed bed	0.5% CO_2 + 1.8% H_2O 20 °C	0.87	[26]
K_2CO_3/Al_2O_3	28.5	Fixed bed	0.5% CO_2 + 1.8% H_2O 20 °C	1.18	[26]
K_2CO_3/5A	11.2	Fixed bed	0.5% CO_2 + 1.8% H_2O 20 °C	0.34	[26]
K_2CO_3/13X	16.2	Fixed bed	0.5% CO_2 + 1.8% H_2O 20 °C	0.53	[26]
K_2CO_3/SG	37.5	Fixed bed	0.5% CO_2 + 1.8% H_2O 20 °C	0.15	[26]
K_2CO_3/AC	15.0	Fixed bed	1% CO_2 + 2% H_2O 60 °C	1.01	[27]
K_2CO_3/AC	33.0	Fixed bed	1% CO_2 + 9% H_2O 60 °C	2.09	[28]
K_2CO_3/AC	24.0	Thermogravimetric Analysis (TGA)	15% CO_2 + 15% H_2O 60 °C	1.67	[29]
K_2CO_3/Al_2O_3	25.0	Bubbling fluidized-bed	13% CO_2 + 13% H_2O 60 °C	1.66	[30]
K_2CO_3/Al_2O_3	35.0	Fluidized bed	13% CO_2 + 9% H_2O 60 °C	1.48	[31]
K_2CO_3/Al_2O_3	30.0	Fixed bed	1% CO_2 + 9 % H_2O 60 °C	1.93	[32]
K_2CO_3/SG	20.5	TGA	1% CO_2 + 2% H_2O 20 °C	0.53	[33]
K_2CO_3/SiO_2	20.0	Fixed bed	1% CO_2 + 2% H_2O 20 °C	1.34	[34]
K_2CO_3/FeOOH	33.0	Fixed bed	1% CO_2 + 2% H_2O 60 °C	1.12	[35]

It is found that the loading characteristics of K_2CO_3 mainly depend on the microscopic characteristics of the support [36], therefore, it is a meaningful work to find the materials with high load capacity for K_2CO_3. Aerogel is a light porous condensed matter with air as the medium, it is a unique nanoporous three-dimensional network structure composed of colloidal particles or polymer molecules that aggregate with each other. It has a very high specific surface area and porosity, with adjustable open pore structure and an easily chemically modified surface, and has a wide range of applications in the field of adsorption [37,38]. At present, research has been widely carried out on SiO_2 aerogel and carbon aerogel in the field of CO_2 adsorption, and the active components are mostly amino groups [39–41]. Linneen et al. [41] prepared the SiO_2-supported tetraethyl pentamine (TEPA) amino-functional CO_2 adsorbent by impregnation method, the TEPA loading capacity can reach 80 wt.%, and the adsorption capacity can reach 6.1 mmol/g at 75 °C under pure CO_2 atmosphere, however, due to the hydrophilicity of the SiO_2 aerogel surface, the structure of the aerogel contracted during the impregnation process. Toufigh et al. [42] prepared K_2CO_3-based CO_2 adsorbent based on Al_2O_3 aerogel prepared by supercritical drying. The aerogel was calcined at 1000 °C to remove surface –OH before impregnation, when the K_2CO_3 loading is 50%, the maximum CO_2 adsorption capacity can reach 7.2 mmol CO_2/g K_2CO_3.

Alumina is a potential support for CO_2 adsorbent, and combining SiO_2 and Al_2O_3 can give aerogel unique advantages. To the best of our knowledge, there are few reports on its research in the field of potassium-based CO_2 adsorbents. At present, the preparation of aerogels by supercritical drying technology (SCD) has achieved commercial application, however, the technology is complicated, with poor safety and high cost. Therefore, the ambient pressure drying technology used for aerogels has attracted much attention [43], which usually reduces the shrinkage and collapse of the skeleton during the drying process through surface modification and other means during the formation of the wet gel. At the same time, in order to make the aerogel suitable for the impregnation process commonly used

in K_2CO_3 load, surface hydrophobic modification treatment is required. The role of the hydrophobic modifier and its effect on CO_2 adsorption performance are currently unclear.

In industrial applications, in addition to a high CO_2 adsorption capacity, the adsorbent should have a fast adsorption rate, which is directly related to the efficiency of the CO_2 capture process. Researchers have conducted in-depth research on the adsorption kinetics of amine-based adsorbents [44,45]. However, there are few studies on the adsorption kinetics of K_2CO_3/Al aerogels [46]. In addition, the stability of the adsorbent during the adsorption-regeneration cycles is also an important indicator in practical industrial applications, so it needs to be investigated.

In this work, potassium-based adsorbents with Al aerogels used as supports were prepared by sol-gel and iso-volume impregnation method. The effects of the microstructures of the supports and the loadings of K_2CO_3 on the adsorption performance and the mechanism were studied. Meanwhile, the pseudo-first order, pseudo-second order, and Avrami's fractional order models were used to fit the adsorption data to study the adsorption rate and adsorption mechanism. Furthermore, the cycle stability of the adsorbents in the continuous adsorption-regeneration process was investigated.

2. Materials and Methods

2.1. Preparation of Adsorbents

Figure 1 is a schematic diagram of the preparation process of the adsorbents. The specific steps are as follows:

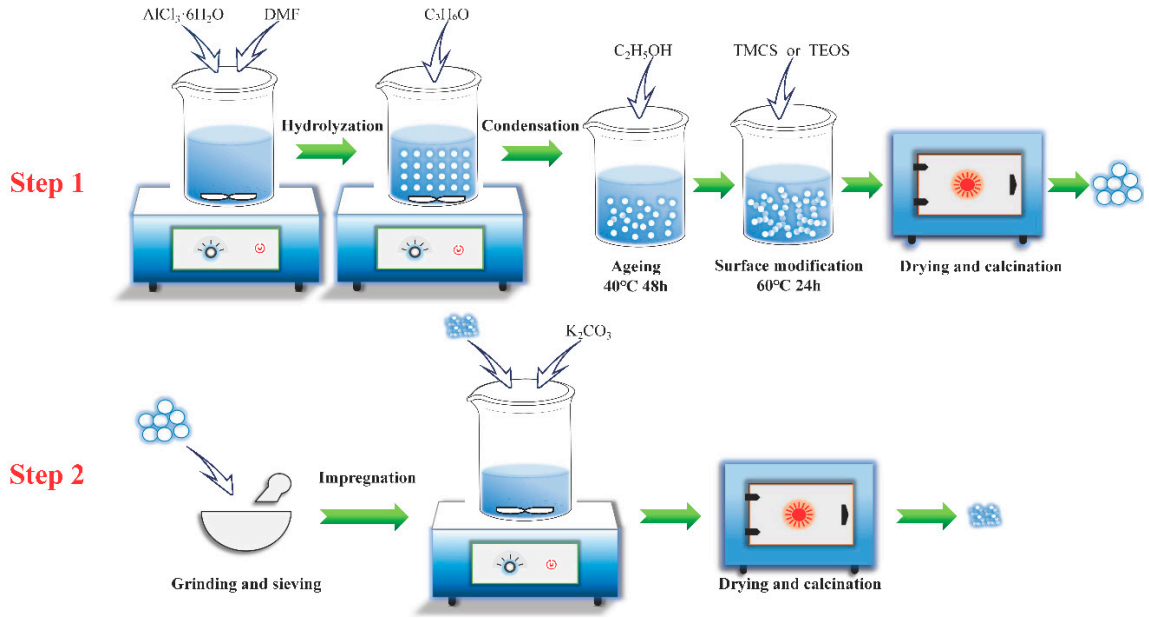

Figure 1. Schematic diagram of the preparation process of adsorbent.

(1) A certain amount of $AlCl_3 \cdot 6H_2O$ (Tianjin Kaitong Chemical Reagent Co., Ltd., Tianjin, China) and *N*,*N*-dimethylformamide (DMF, Tianjin Kaitong Chemical Reagent Co., Ltd., Tianjin, China) were completely dissolved in deionized water; specifically, DMF can control the rate of hydrolysis-polycondensation to improve the uniformity of network channels. Then, propylene oxide (C_5H_6O, Tianjin Fangzheng Reagent Co., Ltd., Tianjin, China) was added to the solution under stirring; specifically, $AlCl_3 \cdot 6H_2O$:H_2O:DMF:C_5H_6O = 1:20:8:0.8 (molar ratio). After the wet gel was formed, it was aged for 48 h at 40 °C in ethanol solution (C_2H_5OH, Tianjin Kaitong Chemical Reagent Co., Ltd., Tianjin, China).

(2) Surface modification was performed on the aged wet gel. The modifiers were ethanol solution (blank control group), 80 wt.% tetraethyl orthosilicate (TEOS, Tianjin Fangzheng Reagent Co., Ltd., Tianjin, China) in ethanol solution (Modifier A) and 80 wt.% trimethyl chlorosilane (TMCS,

Tianjin Fangzheng Reagent Co., Ltd., Tianjin, China) in ethanol solution (Modifier B), respectively. The modification schemes were: no modification, modifier A modification and modifier A and B modification sequentially, respectively. During modification, the wet gel was immersed in the modifier at 60 °C for 24 h.

(3) The modified wet gel was staged drying under ambient pressure, and then calcined at 600 °C for 3 h to obtain Al aerogel, the samples were recorded as Al-B, Al/Si, Al/Si-TMCS according to the modifiers.

(4) The iso-volume impregnation method was used to prepare potassium-based adsorbent. The particle size of the support was selected as 90–120 μm, and the design loading of K_2CO_3 (Nanjing Caiwei Technology Co., Ltd., Nanjing, China) was in the range of 0–40 wt.%. After drying and calcining, the adsorbent was re-sieved to the same size range as the support.

2.2. Experimental Apparatus and Procedure

The CO_2 adsorption experiment was performed in a fixed-bed reaction experiment system. Figure 2 is a simplified diagram of the experimental system. In order to simulate the flue gas environment of the coal-fired power plant, the adsorption atmosphere was selected as 80% N_2 + 10% CO_2 + 10% H_2O. H_2O was controlled by Series III metering pump and was vaporized using electrical heating to the water vapor required for the carbonation reaction. The adsorption process was performed in a quartz tube with an inner diameter of 30 mm and a height of 300 mm, and 3 g adsorbent was placed in the quartz tube. The Xinze S2000 infrared CO_2 detector (Shandong Xinze Technology Co., Ltd., Jinan, China) was used to measure the outlet CO_2 concentration.

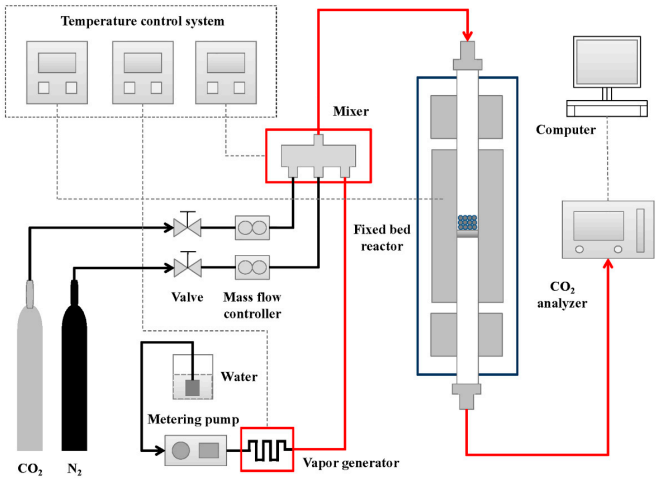

Figure 2. Fixed bed CO_2 adsorption system.

2.3. Data Process

The CO_2 adsorption capacity and K_2CO_3 utilization rate were calculated by Equations (3) and (4), respectively.

$$q = \frac{1000}{m}\left[\int_0^t Q_a\left(\frac{C_{in} - C_{out}}{1 - C_{out}}\right)dt\right]\frac{T_0}{TV_m} \quad (3)$$

$$\eta = \frac{q - q_p}{\alpha / M_{K_2CO_3} \times 1000} \quad (4)$$

where q is the total CO_2 adsorption capacity, mmol/g; q_p is the physical adsorption capacity, mmol/g; C_{in} is the inlet CO_2 concentration, %; C_{out} is the outlet CO_2 concentration, %; Q_a is the gas flow rate, mL/min; m is the mass of the adsorbent, g; t is the adsorption time, min; T is the adsorption temperature, K; T_0 is the gas temperature in standard state, T_0 = 273.15 K; V_m is the molar volume of

gas in standard state, V_m = 22.4 L/mol; α is the actual loading, %; $M_{K_2CO_3}$ is the relative molecular mass of K_2CO_3, $M_{K_2CO_3}$ = 138.

2.4. Characterization Method

An N_2 adsorption-desorption experiment of the adsorbent was performed by ASAP2420 physical adsorption-desorption instrument (Micromeritics Instrument Co., Ltd., Norcross, GA, USA), the specific surface area was calculated by the BET equation, and the pore structure parameters were obtained by the BJH method; Tescan Mira3 scanning electron microscope (SEM, Tescan Co., Ltd., Brno, Czech Republic) was used to characterize the micro-morphology of the adsorbent; phase structure of the adsorbent was characterized by an X/max-2500 X-ray diffractometer (XRD, Rigaku Co., Ltd., Tokyo, Japan) with Cu Kα radiation at a scanning rate of 2°/min over the range of $2° < 2\theta < 85°$. The potassium content of the adsorbent was measured by ARL9800XP X-ray fluorescence spectrometer (XRF, ARL Co., Ltd., Kanton Bern, Switzerland); and the surface groups were analyzed by an IRPrestige-21 Fourier transform infrared (FT-IR, Daojin Co., Ltd., Hongkong, China) spectrometer.

3. Results and Discussion

3.1. Characterization

Figure 3a shows the macroscopic and microscopic surface structures of Al-B, Al/Si and Al/Si-TMCS. The three types of aerogels are translucent solids, Al/Si and Al/Si-TMCS showed larger particles than Al-B, indicating that the ability to stay intact during drying is stronger, while Al-B is broken to a greater extent during ambient pressure drying. SEM results show that Al aerogels obtained under different preparation conditions are all sponge-like structures with relatively uniform pores, which are formed by stacking irregular nanoparticles. and Al-B has a smaller pore size.

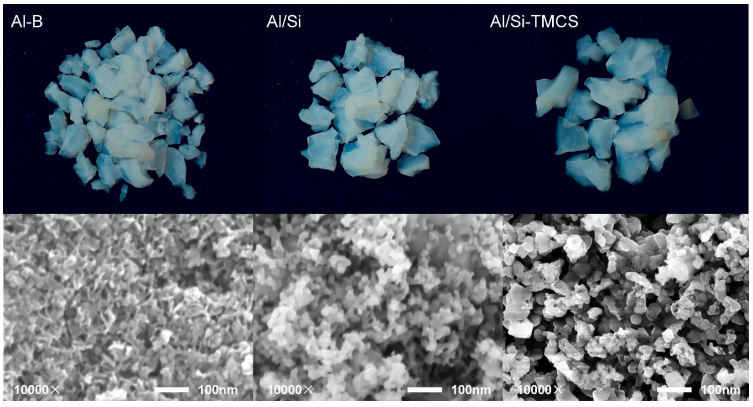

(**a**)

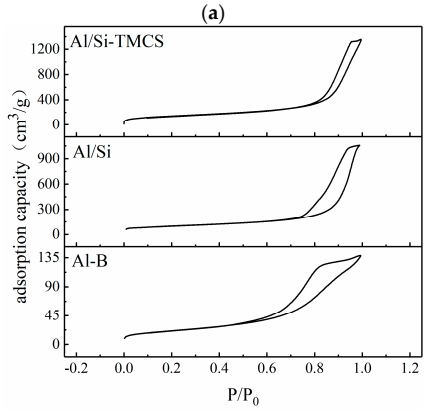

(**b**)

Figure 3. *Cont.*

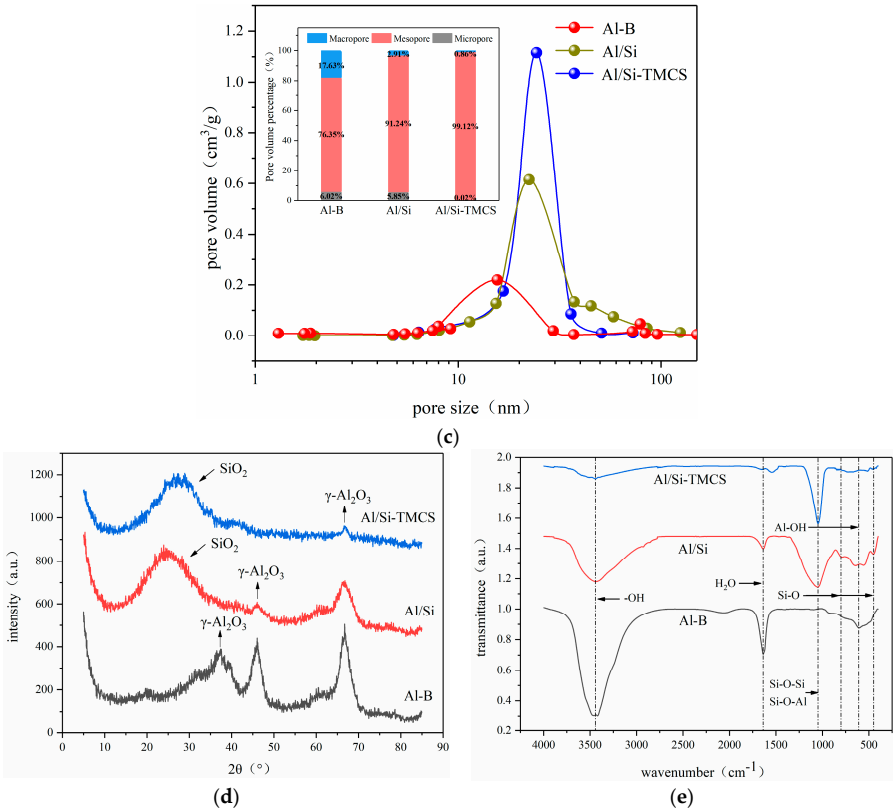

Figure 3. Characterization results of Al_2O_3 aerogels. (**a**) macroscopic and microscopic surface structures of three types of Al aerogels; (**b**) N_2 adsorption-desorption curves of three types of Al aerogels; (**c**) Pore size distributions of three types of Al aerogels; (**d**) X-ray diffraction (XRD) spectra of three types of Al aerogels; (**e**) Fourier transform infrared (FT-IR) spectra of three types of Al aerogels.

Figure 3b,c show the N_2 adsorption-desorption curves and pore size distributions of different samples. According to the classification of the International Union of Pure and Applied Chemistry (IUPAC), the N_2 adsorption-desorption curves of the three adsorbents belong to the typical type IV isotherm. Meanwhile, Al-B has a typical H2 type hysteresis loop, which corresponds to an ink bottle-shaped pore, and the uniformity of the pore structure is relatively poor. Al/Si-TMCS has a typical H1-type hysteresis loop, and the adsorption and desorption branches are steep and almost parallel, indicating the presence of tubular capillary pore with well-organized shape and uniform size. And the hysteresis loop type of Al/Si is between the H1 type and H2 type. It can be seen from the pore size distribution that the pore sizes of the three samples are mainly mesoporous. In particular, the modification of TEOS and TMCS narrowed the pore size distributions of the aerogels, and the proportion of mesopores of Al/Si and Al/Si-TMCS reached more than 90%. A study has shown that a single pore size distribution on the sample surface can make the surface stress more uniform, thereby making it easier for the active component to disperse spontaneously [47]. Al-B has a relatively small pore size, and some micropores and macropores appear, indicating that network shrinkage and structural collapse occur during atmospheric drying and calcination.

The pore structure parameters of the three samples are listed in Table 2. According to Table 2, the maximum specific surface area (635.32 m^2/g) and specific pore volume (2.43 cm^3/g) belong to Al/Si-TMCS, and its specific surface area is higher than that of Al/Si aerogel prepared by Wu [48] using SCD technology (512.50 m^2/g at 600 °C). The specific surface area and specific pore volume of Al-B without TEOS and TMCS modification are 250 m^2/g and 0.49 cm^3/g, respectively, which is much lower than that of Al/Si and Al/Si-TMCS, indicating that TEOS and TMCS play an important role in maintaining the structure of aerogel during ambient drying.

Table 2. Microstructure parameters of the aerogels.

Adsorbents	Specific Surface Area (cm^2/g)	Specific Pore Volume (cm^3/g)	Most Probable Pore Size (nm)
Al-B	250.65 ± 3.21	0.49 ± 0.02	15.6 ± 0.1
Al/Si	496.22 ± 5.43	1.59 ± 0.04	20.4 ± 0.2
Al/Si-TMCS	635.32 ± 5.57	2.43 ± 0.11	26.4 ± 0.2

The XRD spectra of Al aerogels prepared with different modifiers are shown in Figure 3d. The presence of γ-Al_2O_3 is detected in all three samples (2θ = 37°, 46° and 66°), this is formed by the gradual dehydration during the calcination process of the aluminum hydroxide polymer produced by the hydrolysis-polycondensation of the inorganic precursor $AlCl_3 \cdot 6H_2O$. Meanwhile, after being modified by TEOS, the XRD result of Al/Si shows a diffuse peak of amorphous SiO_2 around 2θ = 25°, which indicates that SiO_2 was formed due to the hydrolysis-polycondensation reaction of TEOS during the modification process, and a study has shown that the coating of SiO_2 can strengthen the framework structure of Al_2O_3 aerogel [49]. The modification of TMCS does not have much of an effect on the phase composition of Al/Si aerogel. It is worth noting that γ-Al_2O_3 is more amorphous in Al/Si and Al/Si-TMCS compared to Al-B, which is caused by less –OH on the surface, literature [49] has shown that less –OH can inhibit the transformation of Al_2O_3 from amorphous to crystalline structure at high temperature.

Figure 3e shows the FT-IR spectra of three types of Al aerogels. The strong and wide peak at 3435 cm^{-1} belongs to the stretching vibration of surface-associated hydroxyl group (–OH), and the peak at 1630 cm^{-1} corresponds to the bending vibration of –OH in physically adsorbed H_2O, and the absorption peaks at 882 cm^{-1} and 627 cm^{-1} correspond to Al–OH. –OH is a hydrophilic group, which are prone to occur polycondensation reaction to cause the gel structure to shrink during the drying process of wet gel. The modification of TEOS makes the surface –OH have a certain reduction, at the same time, the vibration of Si–O–Si and Si–O–Al groups appeared at 1095 cm^{-1}, this is because TEOS can undergo a hydrolysis-polycondensation reaction to produce Si–O–Si groups, meanwhile, –OH on the surface of the polycondensation product may also be condensed with Al–OH on the surface of the wet gel to produce Al–O–Si [48]. On the basis of TEOS modification, TMCS can further modify the –OH on the surface of the wet gel, so that the peaks at 3435 cm^{-1} and 1630 cm^{-1} in Al/Si-TMCS almost disappear, which greatly reduces the hydrophilicity of aerogel.

3.2. Loading Characteristics

In order to increase the adsorption capacity and selectivity of Al aerogel for CO_2, K_2CO_3 was loaded with iso-volume impregnation method. The design loadings are selected as 0%, 10%, 20%, 30% and 40%, and the prepared adsorbents were recorded as Al-B-0K, Al-B-10K, Al-B-20K, Al-B-30K, Al-B-40K, Al/Si-0K, Al/Si-10K, Al/Si-20K, Al/Si-30K, Al/Si-40K, Al/Si-TMCS-0K, Al/Si-TMCS-10K, Al/Si-TMCS-20K, Al/Si-TMCS-30K, Al/Si-TMCS-40K. Among them, Al-B-0K, Al/Si-0K and Al/Si-TMCS-0K were used as blank experiments to test the effect of the impregnation process on the structure of the sample. At the same time, they were used to test the water absorption of the support to determine the volume of the K_2CO_3 impregnating solution during the impregnation. The microstructure parameters measured by N_2 adsorption-desorption experiment and the actual K_2CO_3 loading measured by XRF are listed in Table 3.

Affected by the surface –OH, the impregnation process greatly reduces the specific surface area (from 250.65 m^2/g to 140.49 m^2/g) and specific pore volume (from 0.49 cm^3/g to 0.38 cm^3/g) of Al-B, and the pore size becomes smaller, indicating that the impregnation process causes the Al-B framework to shrink. However, the specific surface area (from 635.32 m^2/g to 619.54 m^2/g) and specific pore volume (from 2.43 cm^3/g to 2.39 cm^3/g) of Al/Si-TMCS almost do not change, indicating that it maintains a good structure during the impregnation process. With the increase of the loading, the specific surface area, specific pore volume, and the most probable pore size of Al aerogels under different modification

conditions are continuously decreasing, indicating that more and more K_2CO_3 is filled into the pores, and the change in the content of K in the adsorbents can verify this result. As the theoretical loading increases, the actual K_2CO_3 content in the adsorbent gradually deviates from its theoretical value, indicating that the loading characteristics gradually deteriorate, during the screening process after equal volume impregnation, unloaded K_2CO_3 powder is lost. After loading, the overall pore size distribution of the adsorbents does not change significantly (as shown in Figure 4). The adsorbents are still mesoporous materials, but their most probable pore size has a tendency to become smaller, and their corresponding peak value decreases, which is caused by K_2CO_3 entering the hole.

Table 3. Microstructure parameters of the adsorbents.

Adsorbents	Specific Surface Area (cm^2/g)	Specific Pore Volume (cm^3/g)	Most Probable Pore Size (nm)	Actual Loading (%)
Al-B-0K	140.49 ± 1.87	0.38 ± 0.01	14.1 ± 0.1	0
Al-B-10K	105.41 ± 1.94	0.28 ± 0.01	13.5 ± 0.1	9.1 ± 0.2
Al-B-20K	70.36 ± 1.10	0.15 ± 0.00	12.9 ± 0.1	18.1 ± 0.3
Al-B-30K	40.53 ±1.03	0.09 ± 0.00	10.9 ± 0.1	20.8 ± 0.3
Al-B-40K	10.56 ± 0.86	0.02 ± 0.00	10.1 ± 0.1	27.4 ± 0.4
Al/Si-0K	446.22 ± 4.96	1.39 ± 0.03	19.7 ± 0.2	0
Al/Si-10K	403.26 ± 3.99	1.13 ± 0.02	19.0 ± 0.2	9.8 ± 0.1
Al/Si-20K	353.64 ± 3.64	0.87 ± 0.01	17.8 ± 0.1	18.6 ± 0.1
Al/Si-30K	312.21 ± 3.42	0.69 ± 0.01	16.9 ± 0.2	26.1 ± 0.2
Al/Si-40K	270.55 ± 2.32	0.24 ± 0.01	15.3 ± 0.1	31.9 ± 0.2
Al/Si-TMCS-0K	619.54 ± 5.65	2.39 ± 0.04	26.0 ± 0.2	0
Al/Si-TMCS-10K	578.75 ± 5.12	2.01 ± 0.04	24.1 ± 0.2	9.7 ± 0.1
Al/Si-TMCS-20K	526.74 ± 4.86	1.53 ± 0.02	22.4 ± 0.1	18.9 ± 0.1
Al/Si-TMCS-30K	483.41 ± 4.66	0.96 ± 0.01	19.2 ± 0.1	27.1 ± 0.3
Al/Si-TMCS-40K	420.83 ± 4.21	0.41 ± 0.01	17.8 ± 0.1	33.4 ± 0.2

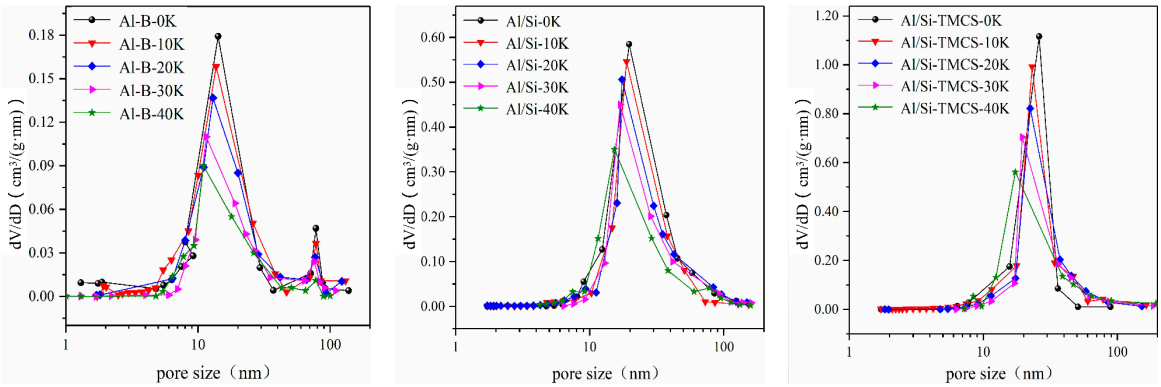

Figure 4. Pore size distribution of the adsorbents after loading.

In order to study the distribution characteristics of K_2CO_3 on different supports, the morphology of the particles was observed using a scanning electron microscope, as shown in Figure 5. In the low loading range, the loose porous structure of the adsorbent can be clearly observed, thus the loading of K_2CO_3 do not have a major impact on the microscopic properties of the supports. As the loading increases, more and more K_2CO_3 enters the pores of the supports, resulting in the surfaces of the adsorbents gradually becoming dense, especially when the theoretical loading reaches 40%. It can be inferred that K_2CO_3 has accumulated on the surface in this case, and the microstructure of the adsorbent deteriorated.

3.3. CO_2 Adsorption Performance

In the presence of water vapor, the potassium-based adsorbent can increase its CO_2 adsorption capacity and selectivity through carbonation. Therefore, the carbonation reaction performance of the adsorbents was studied at 70 °C in 80% N_2 + 10% CO_2 + 10% H_2O. For K_2CO_3 impregnated Al aerogel, its adsorption of CO_2 includes both physical and chemical adsorption, and distinguishing these two types of adsorption is important for the study of adsorption mechanisms. In this work, Hsu's method was used to estimate the physical adsorption capacities of the adsorbents [50]. The specific method is: after the adsorption was saturated, at ambient temperature, the intake gas flow was switched to pure N_2 at 1 L/min, and the vacuum pump connected to the outlet of the quartz tube was turned on (the vacuum was −0.6 bar). When the CO_2 concentration of the outlet of the quartz tube was 0, it could be considered that all physically adsorbed CO_2 had been released, the mass difference of the adsorbent before and after desorption was regarded as the physical adsorption capacity of CO_2. Figure 6 shows the CO_2 adsorption capacities and the calculated utilization rates of K_2CO_3 with different loadings of adsorbents.

The physical adsorption amounts of Al-B, Al/Si and Al/Si-TMCS to CO_2 are 0.49, 0.74 and 0.83 mmol/g, respectively, which shows a positive correlation with specific surface area. This is because a large specific surface area can not only increase the contact area between CO_2 and the adsorbent, but also bring a large number of surface unsaturated adsorption sites. For Al-B-0K, its specific surface area (140.49 m^2/g) is about 1/3 of Al/Si-0K (446.22 m^2/g), but the physical adsorption is not much different from that of Al/Si, which may be related to the more –OH on the surface of Al-B. Deng found that –OH can promote the adsorption of CO_2 [51].

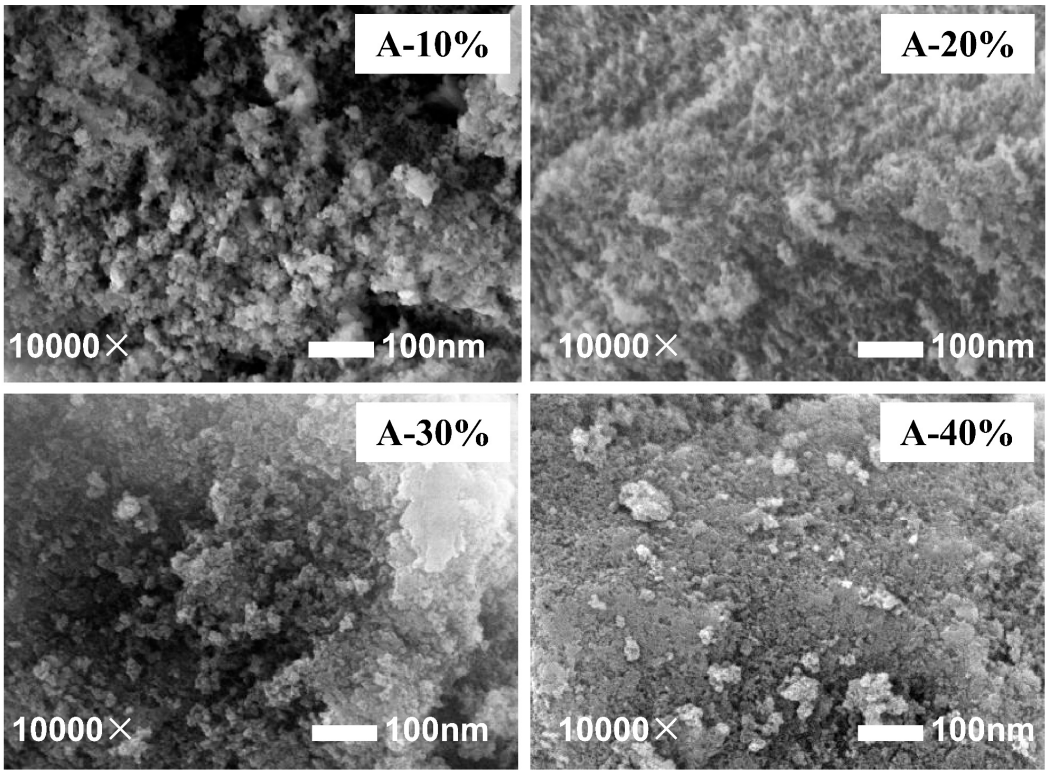

Figure 5. *Cont.*

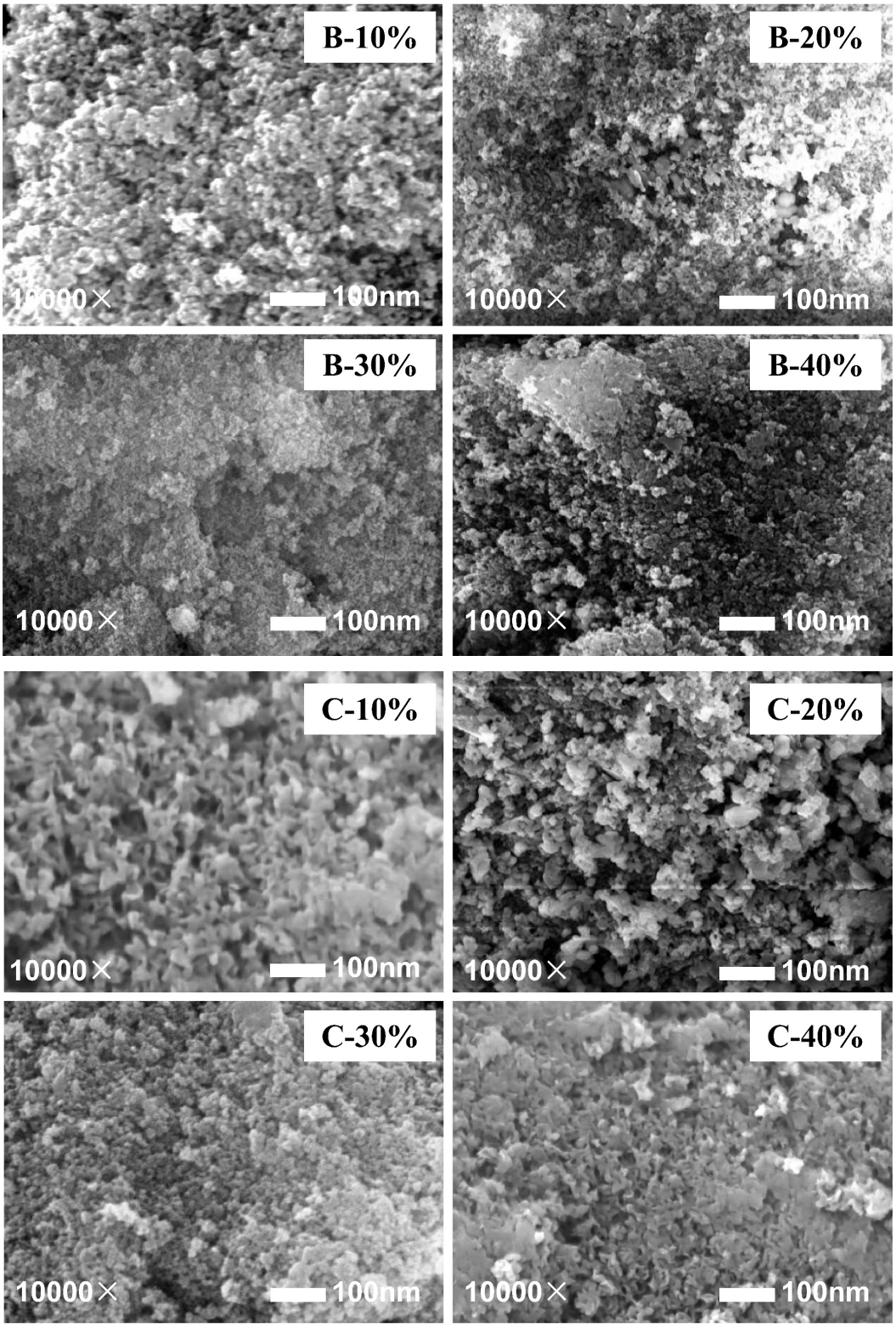

Figure 5. Microstructures of three types of Al aerogels under different loadings. (**A**) Al-B, (**B**) Al/Si, (**C**) Al/Si-TMCS.

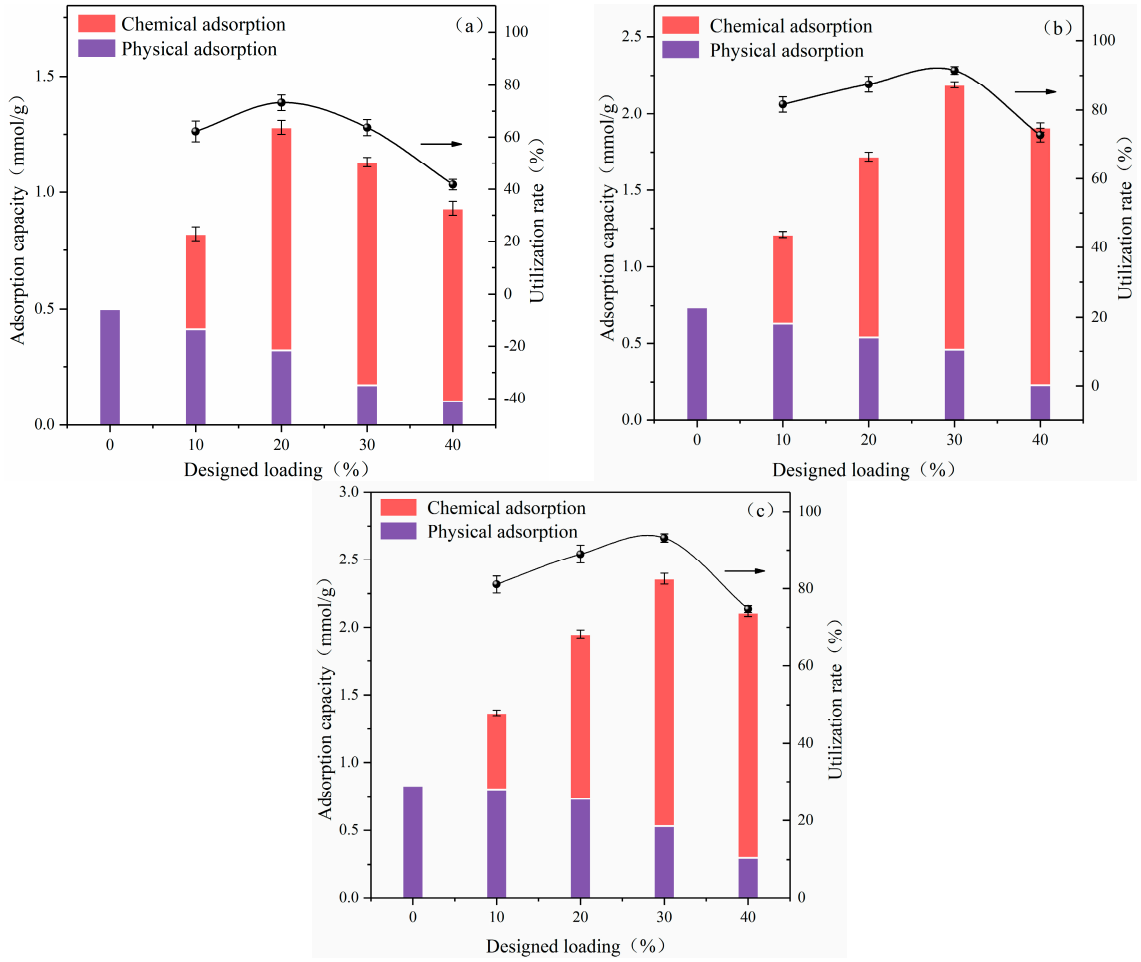

Figure 6. Adsorption capacity of K_2CO_3-based adsorbent under 80% N_2 + 10% CO_2 + 10% H_2O (**a**) Al-B, (**b**) Al/Si, (**c**) Al/Si-TMCS.

Except for 10%, the adsorption processes of CO_2 by adsorbents under different loadings are mainly chemical adsorption. As the loading increases, the contribution of physical adsorption to the entire adsorption process decreases. The physical adsorption capacity of the adsorbents are the smallest when the design loading reaches 40%. This is mainly due to the increasing amount of K_2CO_3 filling the pores of the Al aerogel, resulting in a decrease in the specific surface area and specific pore volume of the adsorbent, which in turn affects the amount of adsorbed CO_2.

In the presence of water vapor, as the loading increases, there is a peak in the CO_2 adsorption capacity result of each type of adsorbent. In the lower loading range, the increase of the loading brings more active sites, which leads to an increase in the amount of adsorption [52]. When the loading is too large, the active components cannot be dispersed uniformly and accumulate. For one thing, the increase of particles leads to a decrease in activity, and for another, the pores are blocked and the resistance to mass transfer is increased, both of them lead to a decrease in the adsorption capacity. Specifically, the adsorption capacity results of Al/Si and Al/Si-TMCS show a peak when the design loading is 30%, while the peak of Al-B appears at 20%. and the peak adsorption capacities are 2.36, 2.22, and 1.27 mmol/g, respectively, its value is higher than the potassium-based adsorbent shown in Table 1. In industrial applications, high adsorption capacity can reduce the adsorption cost by reducing the amount of adsorbent and the size of the equipment. The difference in the positions of the peaks of the three types of adsorbents is due to the different loading characteristics of the three supports for K_2CO_3. Al-TMCS and Al-TEOS have a relatively ordered single mesoporous structure, and the specific surface area and specific pore volume are sufficiently large, so that K_2CO_3 has a larger dispersion threshold

on the surface; while the specific surface area and specific pore volume of Al-B are smaller, and it has a wide pore size distribution with an ink bottle-like pore structure, these factors cause K_2CO_3 to reach the dispersion threshold and start enrichment at a lower loading, resulting in increased grain size and increased mass transfer resistance, which in turn reduces its activity during the carbonation reaction. The utilization rate of K_2CO_3 has the same trend as the amount of CO_2 adsorption, which can also be explained by the above mechanism. The maximum K_2CO_3 utilization rates of the three types of adsorbents are 74.1%, 91.1%, and 93.2%, respectively. This difference may be due to the different particle sizes of K_2CO_3 on the surface and the different optimal carbonation reaction temperatures caused by different activities of different particle sizes of K_2CO_3 [53].

3.4. Adsorption Mechanism

In order to obtain the CO_2 adsorption mechanism of K_2CO_3-based Al aerogels, FT-IR analysis was carried out on Al-B-20K, Al/Si-30K and Al/Si-TMCS-30K, and XRD analysis was carried out on Al-B-20K, Al/Si-30K and Al/Si-TMCS-30K adsorbed in 10% CO_2 + 90%N_2, 10% H_2O + 90% N_2 and 10% H_2O + 10% CO_2 + 80% N_2 atmosphere, respectively, as shown in Figures 7 and 8.

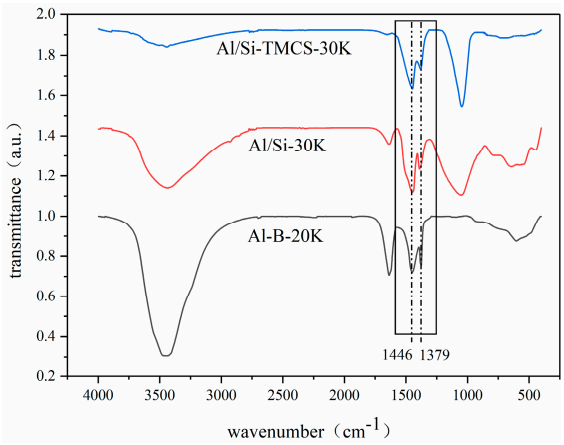

Figure 7. FT-IR spectra of the adsorbents after loading.

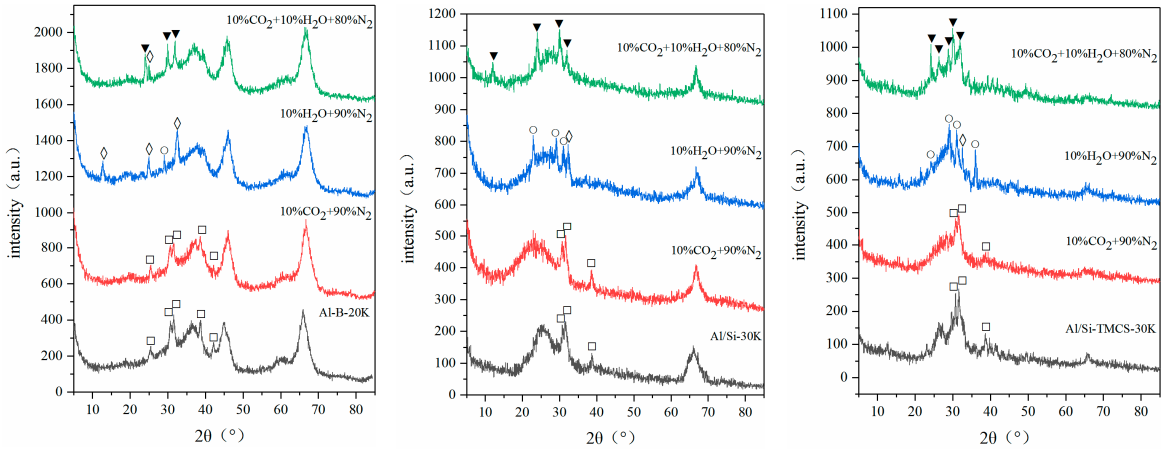

Figure 8. XRD spectra of K_2CO_3-based adsorbent in different atmospheres. □ —K_2CO_3, ◊—K_2CO_3·1.5 H_2O, o—$K_4H_2(CO_3)_3$·1.5 H_2O, ▼—$KHCO_3$.

After loading, peaks related to K_2CO_3 (1446 cm^{-1} and 1379 cm^{-1}) appear in the FT-IR spectra, other surface functional groups do not change significantly, indicating that K_2CO_3 does not affect the surface properties of the supports. According to XRD, only K_2CO_3 peaks appear in the adsorbent after loading, and the peak shape of the supports do not change significantly. This shows that K_2CO_3 exists

on the surface of the support by physical action, no chemical reaction occurs, and the skeleton of the support does not change. After adsorption in 10% CO_2 + 90% N_2, the composition of the three samples do not change, indicating that the adsorbent adsorbs CO_2 by physical action under this condition. After being adsorbed in 10% H_2O + 90% N_2 atmosphere, K species mainly exist as K_2CO_3·1.5 H_2O and $K_4H_2(CO_3)_3$·1.5 H_2O on Al aerogels, this is consistent with Guo's research [54], in particular, the peak of K_2CO_3·1.5 H_2O is stronger in Al-B-20K, which is mainly due to the strong hydrophilicity of Al-B-20K. In 10% H_2O + 10% CO_2 + 80% N_2, K species are mainly $KHCO_3$ after adsorption, indicating that most of the K_2CO_3 undergoes carbonation to generate $KHCO_3$, and K_2CO_3·1.5 H_2O is also detected in Al-B-20K.

The adsorption process of CO_2 by K_2CO_3-based Al aerogel includes the following steps: (1) H_2O and CO_2 diffuse to the outer surface of the adsorbent; (2) H_2O and CO_2 diffuse to the inner surface of the adsorbent through the channel; (3) H_2O and CO_2 are adsorbed to the solid surface; (4) H_2O and CO_2 react with the active center. In this paper, Al-B-20K has a small specific surface area and specific pore volume with an ink bottle-shaped pore, which hinders the internal diffusion process of H_2O and CO_2, and the $KHCO_3$ product layer is easy to block the pores, these factors are not conducive to the occurrence of a carbonation reaction. In addition, scholars generally believe that there are two possible intermediate products of K_2CO_3 carbonation reaction: K_2CO_3·1.5 H_2O and $K_4H_2(CO_3)_3$·1.5 H_2O, and the surface properties of the support and the distribution characteristics of K_2CO_3 will affect the formation of intermediate products during the carbonation reaction [53–57]. Al-B-20K has strong hydrophilicity, under a watery atmosphere, K_2CO_3 will react with H_2O to generate a large amount of K_2CO_3·1.5 H_2O. In terms of crystal structure, compared with $K_4H_2(CO_3)_3$·1.5 H_2O, K_2CO_3·1.5 H_2O is more difficult to achieve the conversion to $KHCO_3$, and supports with better microscopic properties can promote this conversion [54].However, due to the small specific surface area and specific pore volume of Al-B, the dispersibility of formed K_2CO_3·1.5 H_2O is poor, which makes it more difficult to convert into $KHCO_3$, resulting in the presence of K_2CO_3·1.5 H_2O in Al-B-20K after adsorption in 10% H_2O + 10% CO_2 + 80% N_2, which not only affect the conversion rate of carbonation, but also cause valueless consumption of energy in the regeneration process due to the decomposition of K_2CO_3·1.5 H_2O. The Al/Si-30K and Al/Si-TMCS-30K have a large specific surface area and well-developed pore structure, which provides a suitable channel and place for the diffusion and reaction of H_2O and CO_2. At the same time, due to the well-developed pore structure, the heat generated inside the adsorbent during the carbonation reaction can be taken away in time, thereby avoiding local over-temperature of the adsorbent and affecting the carbonation performance. Therefore, compared with Al-B, Al/Si and Al/Si-TMCS are more suitable as K_2CO_3 supports for CO_2 capture.

3.5. Adsorption Kinetics

Temperature is an important factor that affects the carbonation reaction. In this paper, the CO_2 adsorption kinetics of Al-B-20K, Al/Si-30K and Al/Si-TMCS-30K in the range of 50–80 °C were studied. The experimental results were fitted using pseudo-first order, pseudo-second order, and Avrami's fractional order models. The expressions of the three models are shown in Equations (5)–(7), respectively [58–60]. The cumulative adsorption curve and fitting results at different temperatures are shown in Figure 9, and the obtained kinetic parameters are listed in Table 4.

$$q_t = q_e[1 - \exp(-k_1 t)] \tag{5}$$

where q_t is adsorption capacity per unit mass of adsorbent at time t, g/g; q_e is adsorption capacity per unit mass of adsorbent at equilibrium, g/g; t is the adsorption time, min; k_1 is the pseudo-first order rate Constant, min^{-1}.

$$q_t = \frac{q_e^2 k_2 t}{1 + q_e k_2 t} \tag{6}$$

where k_2 is the pseudo-second order rate constant, gmmol^{-1}min^{-1}.

$$q_t = q_e\left[1 - \exp(-k_A t)^{n_A}\right] \quad (7)$$

where k_A is the Avrami kinetic rate constant, min^{-1}; n_A is the Avrami index, when $n_A = 2$, the reaction conforms to a one-dimensional growth mechanism; when $n_A = 3$, the reaction conforms to a two-dimensional growth mechanism.

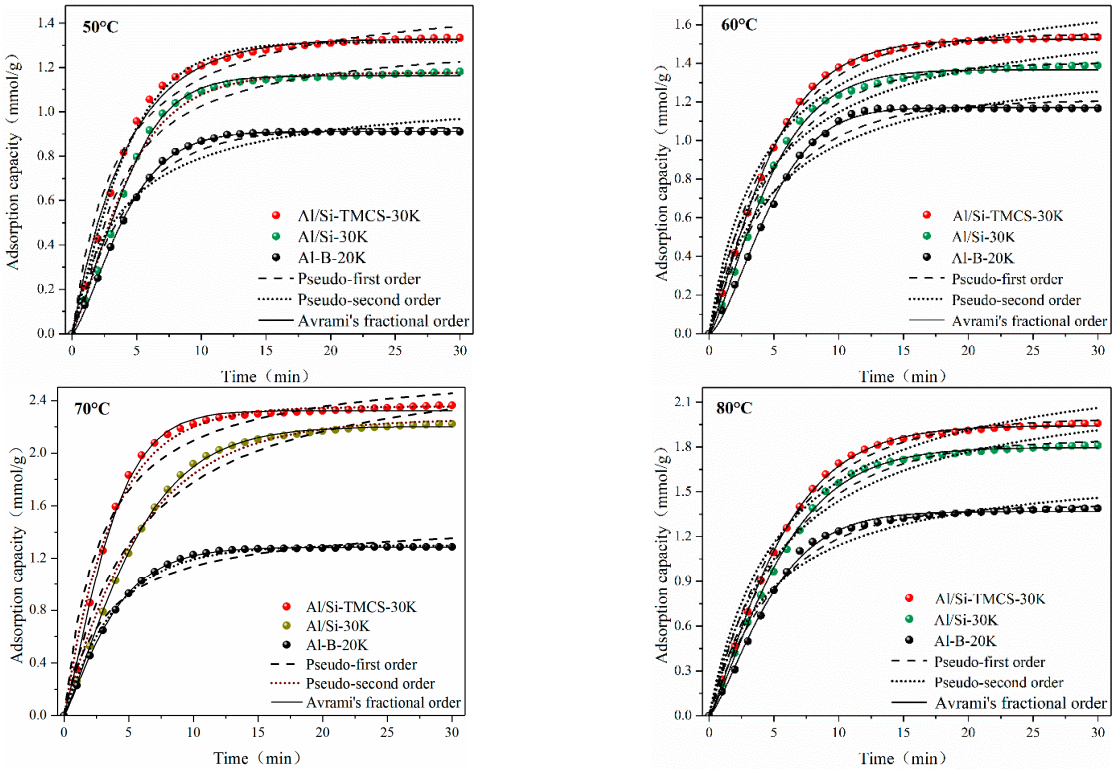

Figure 9. Adsorption kinetics fitting results of adsorbents at different temperatures.

Table 4. The kinetic parameters obtained by different adsorption kinetic models.

Adsorbents	Temperature (°C)	Adsorption Capacity (mmol/g)	Pseudo-First Order			Pseudo-Second Order			Avrami's Fractional Order			
			R^2	k_1	q_e	R^2	k_2	q_e	R^2	k_A	q_e	n_A
Al-B-20K	50	0.91	0.982	0.072	0.93	0.952	0.161	1.06	0.988	0.146	0.87	1.996
	60	1.18	0.979	0.104	1.29	0.967	0.174	1.22	0.991	0.185	1.21	1.984
	70	1.27	0.973	0.135	1.49	0.973	0.185	1.38	0.993	0.219	1.31	2.007
	80	1.37	0.969	0.158	1.46	0.981	0.198	1.43	0.996	0.254	1.39	1.995
Al/Si-30K	50	1.18	0.978	0.154	1.34	0.981	0.162	1.17	0.993	0.184	1.16	1.984
	60	1.39	0.973	0.162	1.60	0.982	0.178	1.38	0.994	0.216	1.36	1.989
	70	2.22	0.969	0.173	2.26	0.985	0.181	2.26	0.995	0.254	2.20	1.996
	80	1.81	0.960	0.1836	2.22	0.985	0.189	1.83	0.994	0.281	1.79	2.011
Al/Si-TMCS-30K	50	1.33	0.973	0.164	1.54	0.979	0.171	1.32	0.993	0.216	1.31	1.985
	60	1.53	0.970	0.176	1.84	0.982	0.185	1.55	0.995	0.234	1.52	1.996
	70	2.36	0.968	0.189	2.45	0.983	0.194	2.32	0.998	0.267	2.35	1.994
	80	1.95	0.963	0.192	2.43	0.984	0.199	1.99	0.998	0.296	1.94	2.001

In the range of 50–80 °C, the adsorption capacity of Al-B-20K shows a gradual increase trend with the increase of temperature, and it reached a maximum of 1.37 mmol/g at 80 °C. However, the adsorption capacities of Al/Si-30K and Al/Si-TMCS-30K gradually increase with the increase of temperature in the low temperature region, and reach a peak when the temperature reaches 70 °C, and then with the rise in temperature, the adsorption capacities have a certain reduction. In the

process of CO_2 adsorption by the adsorbents, physical adsorption and chemical adsorption coexist, and temperature has an important influence on both. In the low temperature region, the increase in temperature is conducive to increasing the activity of the adsorbent, making it easier for the chemical bonds of the active components to be cleaved, which in turn leads to a more prone carbonation reaction. However, when the temperature is too high on the one hand, the increase in temperature is not conducive to the physical adsorption of CO_2 by the adsorbent; on the other hand, an excessively high temperature exacerbates the exothermic effect of the carbonation reaction, which leads to the shift of equilibrium to desorption. For Al/Si-30K and Al/Si-TMCS-30K, due to their better micro characteristics, thermodynamics play a more important role in the process of CO_2 adsorption than kinetics; while Al-B-20K has a poor pore structure, and K_2CO_3 exists as larger particles with a higher crystallinity, which results in higher energy barriers for its active components, and so higher temperature are required to excite its activity.

As can be seen from Figure 9, compared to the pseudo-first order and pseudo-second order models, Avrami's fractional order can better describe the adsorption processes of three adsorbents on CO_2, while the data fitted by the pseudo-first order model shows the largest deviation from the actual data.

In general, the pseudo-first order model is generally suitable for describing the pure physical adsorption of adsorbents at a quite low surface coverage, and regardless of the role of chemical bonds, while the pseudo-second order model is mainly used to describe pure chemical adsorption. At 50 °C, the pseudo-first order model fits Al-B-20K better than the pseudo-second order model, indicating that at this temperature, the carbonation activity of Al-B-20K is not strong, and the physical adsorption of CO_2 by the adsorbent is dominant. As the temperature increases, the correlation coefficient (R^2) obtained by the pseudo-second order model is gradually greater than that of the pseudo-first order model, indicating that the increase of temperature weakens the influence of external mass transfer on the CO_2 adsorption process, and chemical adsorption gradually becomes the speed control step of the entire adsorption process.

In the range of 50–80 °C, the correlation coefficients of pseudo-second order model of Al/Si-30K and Al/Si-TMCS-30K are always larger than pseudo-first order model, which indicates that chemical adsorption always dominates the entire adsorption process. At the same time, as the temperature increases, the influence of chemical adsorption on the entire adsorption process becomes more intense.

Avrami's fractional order model is based on the mechanism of particle nucleation and crystal growth, which is mostly used to explain the complex adsorption mechanism of adsorbate on adsorbent. Among the three models, Avrami's fractional order shows the best fit to the three adsorbents, indicating that the adsorption of CO_2 by the adsorbent is a complex process involving both physical and chemical interactions. It can be seen from the kinetic parameters obtained from the Avrami's fractional order model that as the adsorption temperature increases, the adsorption rate shows a gradually increasing trend. The adsorption rate constant of Al-B-20K is significantly lower than that of the other two adsorbents, which is caused by the poor microstructure of the support and insufficient K_2CO_3 activity on the support surface. At the same time, as the temperature increases, the n_A values are all around 2, indicating that the increase in temperature has not changed the adsorption mechanism of CO_2 on the adsorbent, and the adsorption of CO_2 on the adsorption site conforms to the one-dimensional growth mechanism.

Among the three adsorption kinetic models, Avrami's fractional order model showed the best fitting result, so the Arrhenius equation was used to fit the kinetic parameter k_A to obtain the apparent activation energy of the adsorption process, and the results are shown in Figure 10.

The apparent activation energy of the three adsorbents are 17.38 kJ/mol, 13.55 kJ/mol, and 10.22 kJ/mol, respectively. Compared with Al/Si-30K and Al/Si-TMCS-30K, Al-B-20K shows a higher activation energy, indicating that Al-B-20K requires more energy in the process of CO_2 adsorption, which verifies the above result.

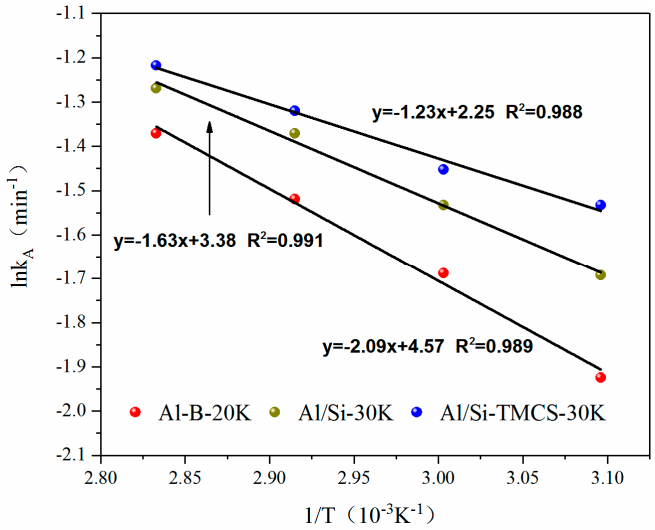

Figure 10. Arrhenius plot of k_A obtained by Avrami's fractional order.

3.6. Cycle Performance of Al/Si-30K and Al/Si-TMCS-30K

In order to have practical value in industrial applications, the CO_2 adsorbent must also have a stable regeneration capacity. In this work, 15 adsorption-regeneration experiments were performed on Al/Si-30K and Al/Si-TMCS-30K, regeneration experiments were carried out at 150 °C in a pure nitrogen atmosphere. The failure mechanisms of the adsorbents were studied through the microstructural changes of the adsorbents during cycling.

The cycling performance of Al-TMCS-30K during the 15 cycles are shown in Figure 11. As the number of cycles increased, the CO_2 adsorption capacity of Al/Si-TMCS-30K showed a slight decrease. After 15 adsorption-regeneration cycles, the adsorption capacity is reduced from only 2.36 mmol/g to 2.21 mmol/g, indicating that it has a good cycle performance, while the reduction of Al/Si-30K reaches 28.4%. During 15 cycles, the microstructure of Al/Si-TMCS-30K has not changed much, while the specific surface area and specific pore volume of Al/Si-30K have decreased to a large extent (as shown in Figure 11b). At the same time, the pore size distribution of Al/Si-30K has changed greatly, and new micropores and macropores have been generated (as shown in Figure 11d). It is speculated that the decrease in the adsorption performance of Al/Si-30K is mainly due to the destruction of the microstructure of the support during the cycles. Since the adsorbents adsorb CO_2 in the water vapor atmosphere, and Al/Si-30K has a certain hydrophilicity, its structure is easily damaged during the continuous water absorption-drying process. On the one hand, the destruction of the support skeleton adversely affects the adsorption and diffusion of CO_2, on the other hand, the collapsed skeleton may wrap K_2CO_3, which hinders the carbonation reaction. The hydrophilicity of Al/Si-TMCS-30K is greatly reduced by TMCS modification, it maintains a good structure in the cycle, so it has a good cycle performance.

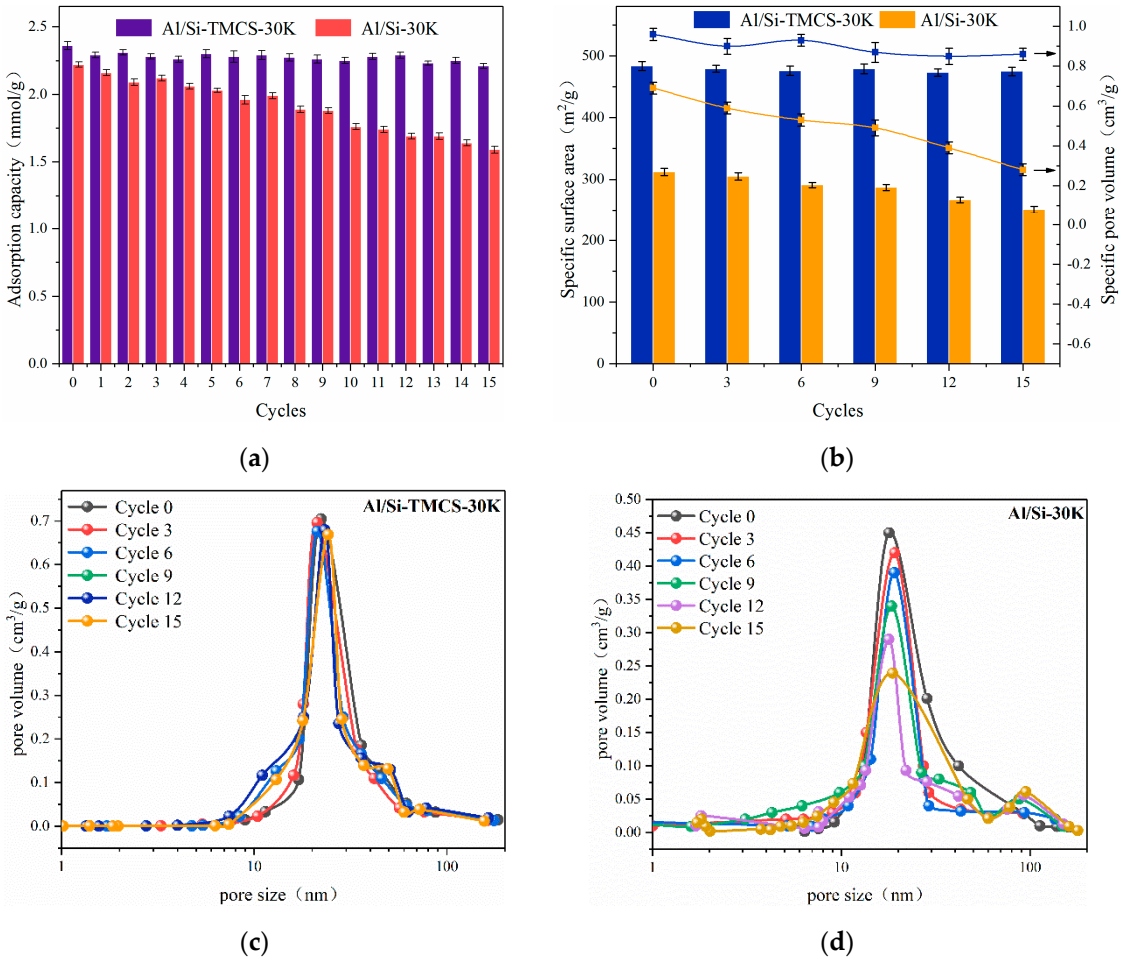

Figure 11. Cycling performance of Al-TMCS-30K and Al-TEOS-30K. (**a**) Adsorption capacity during the cycle. (**b**) Microstructural parameters during the cycle. (**c**) Pore size distribution during the cycle. (**d**) Pore size distribution during the cycle.

4. Conclusions

Aiming at the removal of CO_2 from coal-fired flue gas, a CO_2 adsorbent with Al aerogel used as the support and K_2CO_3 used as the active component was proposed. The effects of surface modifiers and K_2CO_3 loadings on the adsorption characteristics were studied. The main conclusions obtained are as follows:

(1) The modification of TMCS and TEOS during the preparation process can effectively reduce the shrinkage and collapse of the Al aerogel structure by ambient pressure drying, so that it maintains a good microstructure.

(2) TEOS + TMCS-modified Al_2O_3 aerogel shows a best CO_2 adsorption performance at 30% K_2CO_3 loading (Al/Si-TMCS-30K), and the CO_2 adsorption capacity and K_2CO_3 utilization rate are 2.36 mmol/g and 93.2%, respectively.

(3) Avrami's fractional order kinetic model can well fit the CO_2 adsorption process of potassium-based adsorbents, which proves that the adsorption processes of CO_2 by the adsorbents are a complex adsorption mechanism including physical and chemical adsorption. At the same time, from the point of view of adsorption rate constant, compared with common potassium-based adsorbents, Al/Si-TMCS-30K has a faster adsorption kinetics. In the range of 50–80 °C, as the temperature increases, the influence of chemical adsorption on the entire adsorption process increases.

(4) After 15 adsorption-regeneration cycles, the CO_2 adsorption capacity of Al/Si-TMCS-30K remains basically stable, and the microstructure do not change much.

(5) In view of the high CO_2 adsorption capacity, fast adsorption kinetics, and stable regeneration performance of Al/Si-TMCS-30K, it has a great application potential in the field of capturing CO_2 in coal-fired flue gas.

Author Contributions: Conceptualization, Y.J. and Y.W.; methodology, Y.J.; software, B.G.; validation, J.G., M.Z. and H.Y.; formal analysis, Y.W.; investigation, B.G.; resources, J.G., M.Z. and H.Y.; writing—original draft preparation, Y.W.; writing—review and editing, Y.J. and Y.W. All authors have read and agreed to the published version of the manuscript.

Funding: This work was supported by National Natural Science Foundation of China (U1810126, U1910214).

Conflicts of Interest: The authors declare no conflict of interest. The funders had no role in the design of the study; in the collection, analyses, or interpretation of data; in the writing of the manuscript; or in the decision to publish the results.

Abbreviation

TEOS	Tetraethyl orthosilicate
TMCS	Trimethyl chlorosilane
Al-B-20K	Al-B with 20 wt.% K_2CO_3
Al/Si-30K	Al/Si with 30 wt.% K_2CO_3
Al/Si-TMCS-30K	Al/Si-TMCS with 30 wt.% K_2CO_3

References

1. Pacala, S.; Socolow, R. Stabilization wedges: Solving the climate problem for the next 50 Years withcurrent technologies. *Science* **2004**, *305*, 968–972. [CrossRef] [PubMed]
2. Wagner, C.; Esbensen, K.H. A systematic approach to assessing measurement uncertainty for CO_2 emissions from coal-fired power plants-missing contributions from the Theory of Sampling (TOS). *Chem. Eng. Res. Des.* **2011**, *89*, 1572–1586. [CrossRef]
3. Thiruvenkatachari, R.; Su, S.; An, H. Post combustion CO_2 capture by carbon fibre monolithic adsorbents. *Energy Combust. Sci.* **2009**, *35*, 438–455. [CrossRef]
4. Dubois, L.; Thomas, D. Postcombustion CO_2 capture by chemical absorption: Screening of aqueous amine(s)-based solvents. *Energy Procedia* **2013**, *37*, 1648–1657. [CrossRef]
5. Yang, J.; Yu, X.H.; Yan, J.Y. CO_2 Capture Using Amine Solution Mixed with Ionic Liquid. *Ind. Eng. Chem. Res.* **2014**, *53*, 2790–2799. [CrossRef]
6. Sharifzadeh, M.; Shah, N. MEA-based CO_2 capture integrated with natural gas combined cycle or pulverized coal power plants: Operability and controllability through integrated design and control. *J. Clean. Prod.* **2019**, *207*, 271–283. [CrossRef]
7. Jang, D.I.; Park, S.J. Influence of nickel oxide on carbon dioxide adsorption behaviors of activated carbons. *Fuel* **2012**, *102*, 439–444. [CrossRef]
8. Malekbala, M.R.; Soltani, S.; Abdul Rashid, S.; Abdullah, L.C.; Rashid, U.; Nehdi, I.A.; Choong, T.S.Y.; Teo, S.H. Optimization the Process of Chemically Modified Carbon Nanofiber Coated Monolith via Response Surface Methodology for CO_2 Capture. *Materials* **2020**, *13*, 1775. [CrossRef]
9. Chiang, Y.-C.; Chen, Y.-J.; Wu, C.-Y. Effect of Relative Humidity on Adsorption Breakthrough of CO_2 on Activated Carbon Fibers. *Materials* **2017**, *10*, 1296. [CrossRef]
10. Sayari, A.; Belmabkhout, Y.; Serna, R. Flue gas treatment via CO_2 adsorption. *Chem. Eng. J.* **2011**, *171*, 760–774. [CrossRef]
11. Mukherjee1, S.; Sikdar1, N.; Nolan, D. Trace CO_2 capture by an ultramicroporous physisorbent with low water affinity. *Sci. Adv.* **2019**, *9*, 9171–9178. [CrossRef] [PubMed]
12. Gunathilake, C.; Dassanayake, R.S.; Kalpage, C.S.; Jaroniec, M. Development of Alumina-Mesoporous Organosilica Hybrid Materials for Carbon Dioxide Adsorption at 25 °C. *Materials* **2018**, *11*, 2301. [CrossRef] [PubMed]
13. Guo, Y.F.; Li, C.H.; Lu, S.X. K_2CO_3-Modified Potassium Feldspar for CO_2 Capture from Post-combustion Flue Gas. *Energy Fuels* **2015**, *29*, 8151–8156. [CrossRef]
14. Minju, N.; Abhilash, P.; Nair, B.N. Amine impregnated porous silica gel sorbents synthesized from water-glass precursors for CO_2 capturing. *Chem. Eng. J.* **2015**, *269*, 335–342. [CrossRef]

15. Sánchez-Zambrano, K.S.; Lima Duarte, L.; Soares Maia, D.A.; Vilarrasa-García, E.; Bastos-Neto, M.; Rodríguez-Castellón, E.; Silva de Azevedo, D.C. CO_2 Capture with Mesoporous Silicas Modified with Amines by Double Functionalization: Assessment of Adsorption/Desorption Cycles. *Materials* **2018**, *11*, 887. [CrossRef]
16. Wang, P.; Sun, J.; Guo, Y.F. Structurally improved, urea-templated, K_2CO_3-based sorbent pellets for CO_2 capture. *Chem. Eng. J.* **2019**, *374*, 20–28. [CrossRef]
17. Thummakul, T.; Gidaspow, D.; Piumsomboon, P. CFD simulation of CO_2 sorption on K_2CO_3 solid sorbent in novel high flux circulating-turbulent fluidized bed riser: Parametric statistical experimental design study. *Appl. Energy* **2017**, *190*, 122–134. [CrossRef]
18. Lee, S.C.; Kim, J.C. Dry potassium-based sorbents for CO_2 capture. *Catal. Surv. Asia* **2007**, *11*, 171–185. [CrossRef]
19. Lee, S.C.; Chae, H.J.; Choi, B.Y. The effect of relative humidity on CO_2 capture capacity of potassium-based sorbents. *Korean J. Chem. Eng.* **2011**, *28*, 480–486. [CrossRef]
20. Lee, S.C.; Chae, H.J.; Lee, S.J. Development of regenerable MgO-based sorbent promoted with K_2CO_3 for CO_2 capture at low temperatures. *Environ. Sci. Technol.* **2008**, *42*, 2736–2741. [CrossRef]
21. Lee, S.C.; Chae, H.J.; Kwon, Y.M. Characteristics of new potassium-based sorbents prepared with nano-titanium oxide for carbon dioxide capture. *J. Nanoelectron. Optoelectron.* **2010**, *5*, 212–217. [CrossRef]
22. Zhao, C.W.; Chen, X.P.; Zhao, C.S. K_2CO_3/Al_2O_3 for capturing CO_2 in flue gas from power plants, Part 3: CO_2 capture behaviors of K_2CO_3/Al_2O_3 in a bubbling fluidized-bed reactor. *Energy Fuels* **2012**, *26*, 3062–3068. [CrossRef]
23. Zhao, C.W.; Guo, Y.F.; Li, C.H. Carbonation behavior of K_2CO_3/AC in low reaction temperature and CO_2 concentration. *Chem. Eng. J.* **2014**, *254*, 5264–5530. [CrossRef]
24. Zhao, C.W.; Chen, X.P.; Zhao, C.S. K_2CO_3/Al_2O_3 for capturing CO_2 in flue gas from power plants, Part 1: Carbonation behaviors of K_2CO_3/Al_2O_3. *Energy Fuels* **2012**, *26*, 1401–1405. [CrossRef]
25. Zhao, C.W.; Chen, X.P.; Edward, J. Capturing CO_2 in flue gas from fossil fuel-fired power plants using dry regenerable alkali metal-based sorbent. *Prog. Energy Combust. Sci.* **2013**, *3*, 515–534. [CrossRef]
26. Zhao, C.W.; Guo, Y.F.; Li, C. Removal of low concentration CO_2 at ambient temperature using several potassium-based sorbents. *Appl. Energy* **2014**, *124*, 241–247. [CrossRef]
27. Guo, Y.F.; Zhao, C.W.; Li, C.H. CO_2 sorption and reaction kinetic performance of K_2CO_3/AC in low temperature and CO_2 concentration. *Chem. Eng. J.* **2015**, *260*, 596–604. [CrossRef]
28. Lee, S.C.; Choi, B.Y.; Lee, T.J. CO_2 absorption and regeneration of alkali metal-based solid sorbents. *Catal. Today* **2006**, *111*, 385–390. [CrossRef]
29. Zhao, C.W.; Chen, X.P.; Zhao, C.S. CO_2 absorption using dry potassium-based sorbents with different supports. *Energy Fuels* **2009**, *23*, 4683–4687. [CrossRef]
30. Zhao, C.W.; Chen, X.P.; Zhao, C.S. Multiple-cycles behavior of K_2CO_3/Al_2O_3 for CO_2 capture in a fluidized-bed reactor. *Energy Fuels* **2010**, *24*, 1009–1012. [CrossRef]
31. Amiri, M.S.; Shahhosseini, S. Optimization of CO_2 Capture from Simulated Flue Gas Using K_2CO_3/Al_2O_3 in a Micro Fluidized Bed Reactor. *Energy Fuels* **2018**, *32*, 7978–7990. [CrossRef]
32. Lee, S.; Chae, H. Novel regenerable potassium-based dry sorbents for CO_2 capture at low temperatures. *J. Mol. Catal. B-Enzym.* **2009**, *56*, 179–184. [CrossRef]
33. Guo, Y.F.; Zhao, C.W.; Li, C.H. Thermogravimetric analysis of kinetic characteristics of K_2CO_3-impregnated mesoporous silicas in low-concentration CO_2. *J. Therm. Anal. Calorim.* **2015**, *121*, 1393–1402. [CrossRef]
34. Guo, Y.F.; Zhao, C.W.; Sun, J. Facile synthesis of silica aerogel supported K_2CO_3 sorbents with enhanced CO_2 capture capacity for ultra-dilute flue gas treatment. *Fuel* **2018**, *215*, 735–743. [CrossRef]
35. Zhang, B.; Fan, M.; Bland, A. CO_2 separation by a new solid K-Fe sorbent. *Energy Fuels* **2011**, *25*, 1919–1925. [CrossRef]
36. Qin, C.L.; Yin, J.J.; Ran, J.Y. Effect of support material on the performance of K_2CO_3-based pellets for cyclic CO_2 capture. *Appl. Energy* **2014**, *136*, 280–288. [CrossRef]
37. Wang, D.; McLaughlin, E.; Pfeffer, R.; Lin, Y.S. Adsorption of organic compounds in vapor, liquid, nd aqueous solution phases on hydrophobic aerogels. *Ind. Eng. Chem. Res.* **2011**, *50*, 12177–12185. [CrossRef]
38. Francisco, C.; David, F.; Carlos, M. Carbon aerogels from gallic acid-resorcinol mixtures as adsorbents of benzene, toluene and xylenes from dry and wet air under dynamic conditions. *Carbon* **2009**, *47*, 463–469. [CrossRef]

39. Wörmeyer, K.; Smirnova, I. Adsorption of CO_2, moisture and ethanol at low partial pressure using aminofunctionalised silica aerogels. *Chem. Eng. J.* **2013**, *225*, 350–357. [CrossRef]
40. Cui, S.; Cheng, W.; Shen, X. Mesoporous amine-modified SiO_2 aerogel: A potential CO_2 sorbent. *Energy Environ. Sci.* **2011**, *4*, 2070–2074. [CrossRef]
41. Linneen, N.; Pfeffer, R.; Lin, Y.S. CO_2 capture using particulate silica aerogel immobilized with tetraethylenepentamine. *Microporous Mesoporous Mat.* **2013**, *176*, 123–131. [CrossRef]
42. Toufigh Bararpour, S.; Davood, K.; Nader, M. Investigation of the effect of alumina-aerogel support on the CO_2 capture performance of K_2CO_3. *Fuel* **2019**, *242*, 124–132. [CrossRef]
43. Sarawade, P.B.; Kim, J.K.; Kim, H.K.; Kim, H.T. High specific surface area TEOS-based aerogels with largepore volume prepared at an ambient pressure. *Appl. Surf. Sci.* **2007**, *254*, 574–579. [CrossRef]
44. Chen, S.P.; Sun, X.Y.; Luo, X. CO_2 Adsorption on Premodified Li/Al Hydrotalcite Impregnated with Polyethylenimine. *Ind. Eng. Chem. Res.* **2019**, *58*, 1177–1189. [CrossRef]
45. Liu, Q.; Shi, J.J.; Zheng, S.D. Kinetics Studies of CO_2 Adsorption/Desorption on Amine-Functionalized Multiwalled Carbon Nanotubes. *Ind. Eng. Chem. Res.* **2014**, *53*, 11677–11683. [CrossRef]
46. Guo, B.; Wang, Y.; Shen, X.; Qiao, X.; Jia, L.; Xiang, J.; Jin, Y. Study on CO_2 Capture Characteristics and Kinetics of Modified Potassium-Based Adsorbents. *Materials* **2020**, *13*, 877. [CrossRef] [PubMed]
47. Alessandro, D.M.; Smit, B.; Long, J.R. Carbon dioxide capture: Prospects for new materials. *Angew. Chem. Int. Ed.* **2010**, *49*, 6058–6082. [CrossRef] [PubMed]
48. Wu, X.; Shao, G.; Cui, S.; Wang, L.; Shen, X. Synthesis of a novel Al_2O_3-SiO_2 composite aerogel with high specific surface area at elevated temperatures using inexpensive inorganic salt of aluminum. *Ceram. Int.* **2016**, *42*, 874–882. [CrossRef]
49. Miller, J.B.; Ko, E.I. A homogeneously dispersed silica dopant for control of the textural and structural evolution of an alumina aerogel. *Catal. Today* **1998**, *43*, 51–67. [CrossRef]
50. Hsu, S.; Lu, C. Modification of Single-walled Carbon Nanotubes for Enhancing Isopropyl Alcohol Vapor Adsorption from Air Streams. *Sep. Sci. Technol.* **2007**, *42*, 2751–2766. [CrossRef]
51. Deng, H.; Doonan, C.; Furukawa, H. Multiple functional groups of varying ratios in metal-organic frameworks. *Science* **2010**, *327*, 846–850. [CrossRef] [PubMed]
52. Fan, B.-G.; Jia, L.; Wang, Y.-L.; Zhao, R.; Mei, X.-S.; Liu, Y.-Y.; Jin, Y. Study on Adsorption Mechanism and Failure Characteristics of CO_2 Adsorption by Potassium-Based Adsorbents with Different Supports. *Materials* **2018**, *11*, 2424. [CrossRef] [PubMed]
53. Yi, C.-K.; Jo, S.-H.; Seo, Y.; Lee, J.-B.; Ryu, C.-K. Continuous operation of the potassium-based dry sorbent CO_2 capture process with two fluidized-bed reactors. *Int. J. Greenh. Gas Control.* **2007**, *1*, 31–36. [CrossRef]
54. Guo, Y.F.; Zhao, C.W.; Li, C.H. Thermogravimetric analysis of carbonation behaviors of several potassium-based sorbents in low concentration CO_2. *J. Therm. Anal. Calorim.* **2014**, *119*, 441–451. [CrossRef]
55. Adu, E.; Zhang, Y.; Liu, D.; Tontiwachwuthikul, P. Parametric Process Design and Economic Analysis of Post-Combustion CO_2 Capture and Compression for Coal- and Natural Gas-Fired Power Plants. *Energies* **2020**, *13*, 2519. [CrossRef]
56. Zhao, C.W.; Chen, X.P.; Zhao, C.S. Effect of crystal structure on CO_2 capture characteristics of dry potassium-based sorbents. *Chemosphere* **2009**, *75*, 1401–1404. [CrossRef]
57. Abhimanyu, J.; Arturo, G.; Nader, M. Post-combustion CO_2 capture using solid K_2CO_3: Discovering the carbonation reaction mechanism. *Appl. Energy.* **2016**, *179*, 531–543. [CrossRef]
58. Blanchard, G.; Maunaye, M.; Martin, G. Removal of heavy metals from waters by means of natural zeolites. *Water Res.* **1984**, *18*, 1501–1507. [CrossRef]
59. Avrami, M. Kinetics of phase change. I General Theory. *J. Chem. Phys.* **1939**, *7*, 1103–1112. [CrossRef]
60. Singh, V.K.; Kumar, E.A. Comparative studies on CO_2 adsorption kinetics by solid adsorbents. *Energy Procedia* **2016**, *90*, 316–325. [CrossRef]